Magnetic Properties Diagnostic for the Existence of Iron(II)-Iron(II) Bonds in Dinuclear Complexes Which Derive from Stepwise Insertion Reactions on Unsupported Iron-Aryl Bonds

Alain Klose,[†] Euro Solari,[†] Carlo Floriani,*[,†] Angiola Chiesi-Villa,[‡] Corrado Rizzoli,[‡] and Nazzareno Re[§]

Contribution from the Institut de Chimie Minérale et Analytique, BCH 3307, Université de Lausanne, CH-1015 Lausanne, Switzerland, Istituto di Strutturistica Chimica, Centro di Studio per la Strutturistica Diffrattometrica del CNR, Università di Parma, I-43100 Parma, Italy, and Dipartimento di Chimica, Università di Perugia, I-06100 Perugia, Italy

Received March 14, 1994[⊕]

Abstract: Several iron-aryl complexes have been considered for studying iron-aryl carbon bonds: $[Fe_2Mes_4]$ (**1**, Mes = 2,4,6-$Me_3C_6H_2$); $[Fe_2(2,4,6\text{-}Pr^i_3C_6H_2)_4]$ (**2**), and $[Py_2FeMes_2]$ (**3**, Py = pyridine). The first one, however, is the most accessible on a large scale and thus has been used in our exploratory work on insertion reactions. The reaction of **1** with Bu^tNC led to the dimeric homoleptic iminoacyl complex $[\{\eta^2\text{-}C(Mes)=NBu^t\}_2Fe_2\{\mu\text{-}C(Mes)=NBu^t\}_2]$ (**4**), containing a very short Fe-Fe distance [2.371(4) Å]. The iron-carbon bonds present in complex **4** reacted further, inserting CO_2 and CyN=C=NCy [Cy = C_6H_{11}] and leading to the monomeric complexes $[\{OC(O)C(Mes)=NBu^t\}_2Fe]$ (**5**) and $[\{CyNC(=NCy)C(Mes)=NBu^t\}_2Fe]$ (**6**). For complexes **5** and **6**, respectively, the original iron-aryl carbon bond has been functionalized twice by a successive insertion of Bu^tNC and a cumulene. In the reaction with PhCN, only the bridging mesityl inserted the nitrile functionality to give $[(PhCN)_2(Mes)_2Fe_2\{\mu\text{-}N=C(Mes)(Ph)\}_2]$ (**7**). Complex **7** contains a bridging imino group and has a rather long Fe-Fe distance [2.859(2) Å]. The unreacted terminal mesityl group in **7** has been engaged in other insertion reactions, *i.e.* with CyN=C=NCy and PhNCO. In the resulting dimeric compounds $[\{CyNC(Mes)=NCy\}_2Fe_2\{\mu\text{-}N=C(Mes)(Ph)\}_2]$ (**8**), and $[\{OC(Mes)=NPh\}_2Fe_2\{\mu\text{-}N=C(Mes)(Ph)\}_2]$ (**9**), the $[Fe_2\{\mu\text{-}N=C(Mes)(Ph)\}_2]$ bimetallic core is conserved and the magnetic properties are very close to those of **7**. In complex **10**, $[\{(Mes)(Ph)C=N\}_2Fe_2\{\mu\text{-}C(Mes)=NBu^t\}_2]$, derived from the reaction of **7** with Bu^tNC, the iminoacyl replaces the imino group as bridging ligand. This conclusion is strongly supported by the magnetic analysis. All of the iron(II)-iron(II) dimers reported here have strongly reduced magnetic moments. A detailed analysis of the magnetic susceptibility as a function of the temperature allowed us to make a clear distinction between antiferromagnetic couplings and the presence of a metal-metal bond. Crystallographic details are as follows: **2** is monoclinic; space group $C2$; a = 26.154(7), b = 12.868(6), c = 19.476(6) Å; β = 108.06(4)°; Z = 4; and R = 0.057. **3** is monoclinic; space group $P2_1/n$; a = 8.190(1), b = 22.141(3), c = 14.674(3) Å; β = 102.52(4)°; Z = 4; and R = 0.061. **4** is monoclinic; space group $P2/n$; a = 15.879(2), b = 10.865(1), c = 18.126(3) Å; β = 108.52(2)°; Z = 2; and R = 0.038. **6** is triclinic; space group $P\bar{1}$; a = 14.476(2), b = 16.378(2), c = 12.122(1) Å; α = 90.31(1)°, β = 111.74(2)°, γ = 93.12(1)°; Z = 2; and R = 0.051. **7** is triclinic; space group $P\bar{1}$; a = 12.680(3), b = 13.510(3), c = 10.870(5) Å; α = 107.63(2)°, β = 104.30(3)°, γ = 67.00(2)°; Z = 1; and R = 0.060.

Introduction

The metal-carbon bond in homoleptic alkyl- and aryl-metal derivatives, especially when they occur as aggregates, experiences a chemical environment similar to that proposed for a hydrocarbon interacting with a metal surface.[1] This study focuses on the chemistry of the dimer $[Fe_2Mes_4]$ (Mes = 2,4,6-$Me_3C_6H_2$) containing two terminal and two bridging mesityl groups.[2] The availability of $[Fe_2Mes_4]$ facilitates chemical and physical studies,[3] and this is particularly relevant since the iron-carbon bond is ubiquitous in metal-assisted organic transformations.[4,5] Herein, we report an investigation on the insertion reactions of **1** with a number of substrates which allowed us to achieve three major goals.

(i) We obtained homoleptic organometallic derivatives of iron(II) containing functionalized aryl substituents. Additionally, in some cases a polyinsertion reaction has been observed, thus introducing two different functional groups[6] in the appropriate sequence in a single iron-carbon bond of $[Fe_2Mes_4]$.

* To whom correspondence should be addressed.
† Université de Lausanne.
‡ Università di Parma.
§ Università di Perugia.
⊕ Abstract published in *Advance ACS Abstracts*, September 1, 1994.

(1) *Selective Hydrocarbon Activation*; Davies, J. A., Watson, P. L., Leibman, J. F., Greenberg, A., Eds.; VCH: New York, 1990. Gates, B. C. In *Catalyst Design*; Wiley: New York, 1987. Campbell, I. M. *Catalysis and Surfaces*; Chapman and Hall: London, U.K., 1988. *Homogeneous Transition Metal Catalyzed Reactions*; Moser, W. R., Slocum, D. W., Eds.; ACS 230; American Chemical Society: Washington, DC, 1992.

(2) (a) Machelett, B. Z. *Chem.* **1976**, *16*, 116. (b) Muller, H.; Seidel, W.; Görls, H. *J. Organomet. Chem.* **1993**, *445*, 133.

(3) (a) Eisen-Organische Verbindugen (Organic Iron Compounds). *Gmelin Handbook of Inorganic Chemistry*; 1976; Vol. 36, Part B, pp 6-15. (b) Davison, P. J.; Lappert, M. F.; Pearce, R. *Chem. Rev.* **1976**, *76*, 219. (c) Johnson, M. D. Mononuclear Iron Compounds with η^1-Hydrocarbon Ligands. In *Comprehensive Organometallic Chemistry*; Wilkinson, G., Stone, F. G. A., Abel, E. W., Eds.; Pergamon: Oxford, U.K., 1982; Vol. 4, Chapter 31.2.

(4) (a) Pearson, A. J. In *Advances in Metal-Organic Chemistry*; JAI Press: London, U.K., 1989; Vol. 1, pp 1-35. (b) Davies, S. G. *Organotransition Metal Chemistry: Applications to Organic Synthesis*; Pergamon: New York, 1986. (c) Pearson, A. J. In *Comprehensive Organometallic Chemistry*; Wilkinson, G., Stone, F. G. A., Abel, E. W., Eds.; Pergamon: Oxford, U.K., 1982; Vol. 8, Chapter 58. (d) *The Organic Chemistry of Iron*; Koerner von Gustorf, E. A., Grevels, F. W., Fischler, I., Eds.; Academic: Orlando, FL, 1978; 1981. See also earlier reviews cited in these articles. (e) Reetz, M. T.; Stanchev, S. *J. Chem. Soc., Chem. Commun.* **1993**, 328.

(5) (a) Liebeskind, L. S.; Welker, M. E.; Fengl, R. W. *J. Am. Chem. Soc.* **1986**, *108*, 6328. (b) Davies, S. G. *Pure Appl. Chem.* **1988**, *60*, 13. Davies, S. G. *Chem. Br.* **1989**, 268.

0002-7863/94/1516-9123$04.50/0 © 1994 American Chemical Society

Table 1. Experimental Data for the X-ray Diffraction Studies on Crystalline Compounds 2–4, 6, and 7

compound	2	3	4	6	7
chemical formula	$C_{60}H_{92}Fe_2 \cdot C_6H_6$	$C_{28}H_{32}FeN_2$	$C_{56}H_{80}Fe_2N_4 \cdot C_6H_{14}$	$C_{54}H_{84}FeN_6$	$C_{64}H_{64}Fe_2N_4 \cdot 2(C_6H_6)$
a (Å)	26.154(7)	8.190(1)	15.879(2)	14.476(2)	12.680(3)
b (Å)	12.868(6)	22.141(3)	10.865(1)	16.378(2)	13.510(3)
c (Å)	19.476(6)	14.674(3)	18.126(3)	12.122(1)	10.870(5)
α (deg)	90	90	90	90.31(1)	107.63(2)
β (deg)	108.06(4)	102.52(4)	108.52(2)	111.74(2)	104.30(3)
γ (deg)	90	90	90	93.12(1)	67.00(2)
V (Å)^3	6232(4)	2597.6(8)	2965.3(8)	2664.6(7)	1615.9(10)
Z	4	4	2	2	1
fw	1003.2	452.4	1007.2	873.2	1157.2
space group	$C2$ (5)	$P2_1/n$ (14)	$P2/n$ (13)	$P\bar{1}$ (2)	$P\bar{1}$ (2)
t (°C)	22	22	22	22	22
λ (Å)	0.71069	0.71069	0.71069	0.71069	0.71069
ρ_{calcd} (g cm^{-3})	1.069	1.157	1.128	1.088	1.189
μ (cm^{-1})	4.98	5.94	5.26	3.18	4.91
transmn coeff	0.926–1.000	0.972–1.000	0.969–1.000	0.932–1.000	0.935–1.000
R^a	0.057	0.061	0.038	0.051	0.060
Rw^b	0.061	0.072	0.044	0.058	0.069

$^a R = \Sigma||\Delta F|/\Sigma|F_o|$. $^b R_w = \Sigma w^{1/2}|\Delta F|/\Sigma w^{1/2}|F_o|$.

(ii) We showed different reactivity for the bridging *vs* the terminal mesityl in terms of migratory aptitude. Some substrates react with the bridging aryl while the terminal one remains untouched and available for subsequent engagement in insertion reactions with a different substrate. This sequence allows the selective functionalization of both the terminal and the bridging iron–carbon bonds.

(iii) We studied the magnetic properties of a class of relevant dimeric iron(II) complexes. The magnetic study is, much more so than the iron–iron bond distance, diagnostic for the presence or the absence of a metal–metal bond. Preliminary results have been communicated earlier.[7]

Results and Discussion

The iron(II)–aryl carbon bond is now available in the form of dimers **1** and **2** in the absence of any ancillary ligand.

$$2\ FeCl_2.(THF)_{1.5} + 4\ ArMgBr \xrightarrow[\text{dioxane}]{THF}$$

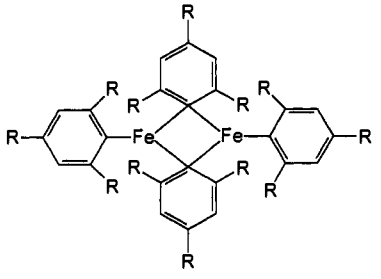

(1)

R = Me, [Fe_2Mes_4], [Mes = 2,4,6-$Me_3C_6H_2$], **1**

R = Pr^i, [Fe_2(2,4,6-$Pr^i_3C_6H_2)_4$], **2**

The synthesis of **1** was reported several years ago[2a] and its dimeric structure was analyzed only very recently.[2b] For synthetic purposes, however, we improved and scaled up the synthesis of **1** (see Experimental Section). The introduction of a significantly hindered Pr^i instead of Me group on the phenyl ring did not break down the dimeric structure as we observed in the X-ray analysis reported in Figure 1. The structure of **2** is very close to that of **1**, with a slight difference in the Fe···Fe distance [Fe···Fe, 2.614(1) Å, **1**; 2.666(3) Å, **2**]. In such cases, the question of the existence or not of an iron–iron bond will be based on the magnetic properties of a number of related dimers which we reported in this paper.

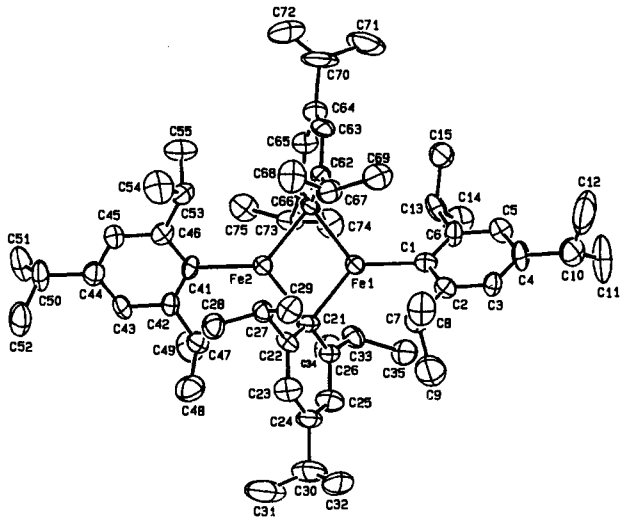

Figure 1. ORTEP drawing for complex **2** (30% probability ellipsoids).

The structure of **2** consists of dimeric units (Figure 1) and benzene solvent molecules in a complex/solvent molar ratio of 1/1. Selected bond distances and angles are listed in Table 7. The two iron atoms are bridged by two aryl ligands and a terminal aryl completes the trigonal coordination around each iron. The metal atoms lie in the plane of the coordinated carbon atoms, the out-of-plane distance being 0.022(2) and 0.017(2) Å for Fe1 and Fe2, respectively. The two coordination planes are coplanar, the dihedral angle between them being 1.6(2)°. The geometry, as well as the conformation of the whole molecule is very similar to that observed in Fe_2Mes_4.[2b] The significant lengthening observed for the Fe–C bond distances as well as for the Fe1···Fe2 distance with respect to those in Fe_2Mes_4 has to be related to the bulky substituents on the aromatic rings. The bridging aromatic rings are mutually oriented to make a dihedral angle of 42.1(3)°, and the terminal C1···C6 and C41···C46 rings form a dihedral angle of 83.5(3)°. They are twisted by 40.2(3)° and 43.1(3)° with respect to the coordination plane around Fe1 and Fe2, respectively. The Fe1 and Fe2 atoms are 0.092(2) and 0.119(3) Å from the C1···C6 and C41···C46 rings, respectively. The *o*-isopropyl substituents are oriented in such a way to bring the α-hydrogen atoms close to the iron atoms. In particular, the H atoms of the terminal ligands (H7, H13, H47, H53) approach the Fe1 and Fe2 iron atom at distances ranging from 2.62 to 2.69 Å. The H atoms of the bridging ligand approach more closely: Fe1···H33 = 2.26 Å, Fe1···H67 = 2.41 Å, Fe2···H27 = 2.33 Å, Fe2···H73 = 2.34

(6) (a) Vivanco, M.; Ruiz, J.; Floriani, C.; Chiesi-Villa, A.; Rizzoli, C. *Organometallics* **1993**, *12*, 1794. (b) Ruiz, J.; Vivanco, M.; Floriani, C.; Chiesi-Villa, A.; Rizzoli, C. *Organometallics* **1993**, *12*, 1802. (c) Vivanco, M.; Ruiz, J.; Floriani, C.; Chiesi-Villa, A.; Rizzoli, C. *Organometallics* **1993**, *12*, 1811.

(7) Klose, A. K.; Solari, E.; Ferguson, R.; Floriani, C.; Chiesi-Villa, A.; Rizzoli, C. *Organometallics* **1993**, *12*, 2414.

Table 2. Fractional Atomic Coordinates (×10⁴) for Complex **2**

atom	x/a	y/b	z/c	atom	x/a	y/b	z/c
Fe1	1534.3(7)	0(–)	–2231.8(9)	C43	2579(3)	4156(6)	–3654(5)
Fe2	2098.1(7)	1526.0(18)	–2579.3(9)	C44	3061(3)	4490(6)	–3161(5)
C1	1112(3)	–1192(6)	–1925(5)	C45	3276(3)	3962(6)	–2509(5)
C2	713(3)	–963(6)	–1610(5)	C46	3008(3)	3100(6)	–2351(5)
C3	449(3)	–1765(6)	–1376(5)	C47	1789(6)	3005(12)	–4052(8)
C4	584(3)	–2797(6)	–1457(5)	C48	1363(7)	3822(18)	–4133(9)
C5	983(3)	–3026(6)	–1772(5)	C49	1841(8)	2729(16)	–4783(9)
C6	1247(3)	–2224(6)	–2006(5)	C50	3367(7)	5445(13)	–3304(9)
C7	541(6)	138(14)	–1516(8)	C51	3641(8)	5253(13)	–3866(10)
C8	578(8)	372(15)	–764(11)	C52	3047(8)	6412(15)	–3442(12)
C9	–32(9)	342(18)	–2029(15)	C53	3249(5)	2547(13)	–1634(8)
C10	297(8)	–3684(16)	–1212(12)	C54	3420(8)	3316(17)	–1008(8)
C11	80(11)	–4508(18)	–1768(13)	C55	3720(7)	1884(17)	–1677(10)
C12	590(13)	–4148(32)	–621(20)	C61	2393(3)	46(7)	–2068(4)
C13	1651(7)	–2532(12)	–2379(8)	C62	2605(3)	–153(7)	–1330(4)
C14	1425(7)	–3175(17)	–3031(10)	C63	3063(3)	–770(7)	–1070(4)
C15	2125(6)	–3096(14)	–1827(10)	C64	3309(3)	–1189(7)	–1549(4)
C21	1233(3)	1464(7)	–2739(5)	C65	3097(3)	–990(7)	–2287(4)
C22	1146(3)	2365(7)	–2392(5)	C66	2639(3)	–372(7)	–2547(4)
C23	669(3)	2924(7)	–2670(5)	C67	2347(6)	290(14)	–785(8)
C24	279(3)	2581(7)	–3295(5)	C68	2690(8)	1086(15)	–282(8)
C25	366(3)	1680(7)	–3642(5)	C69	2185(7)	–583(17)	–365(8)
C26	843(3)	1122(7)	–3364(5)	C70	3803(9)	–1893(24)	–1258(13)
C27	1560(5)	2808(11)	–1708(8)	C71	3690(10)	–2952(20)	–1153(16)
C28	1711(6)	3909(12)	–1807(8)	C72	4260(9)	–1399(24)	–808(20)
C29	1375(6)	2703(13)	–1042(8)	C73	2450(5)	–195(12)	–3344(7)
C30	–250(8)	3196(19)	–3623(13)	C74	2218(7)	–1178(14)	–3782(8)
C31	–178(10)	4177(30)	–3880(15)	C75	2882(7)	285(13)	–3663(8)
C32	–582(7)	3170(17)	–3125(14)	C81	4130(14)	1782(15)	5171(8)
C33	895(5)	159(12)	–3752(7)	C82	4621(14)	1887(15)	5715(8)
C34	972(7)	346(13)	–4500(8)	C83	4635(14)	2242(15)	6397(8)
C35	438(6)	–619(13)	–3830(8)	C84	4157(14)	2493(15)	6535(8)
C41	2526(3)	2767(6)	–2844(5)	C85	3666(14)	2388(15)	5992(8)
C42	2311(3)	3295(6)	–3496(5)	C86	3653(14)	2033(15)	5310(8)

Table 3. Fractional Atomic Coordinates (×10⁴) for Complex **3**

atom	x/a	y/b	z/c	atom	x/a	y/b	z/c
Fe	1696.3(15)	1757.7(6)	1394.1(8)	C15	5407(6)	346(2)	1346(4)
N1	–15(9)	1415(4)	153(5)	C16	4270(6)	822(2)	1132(4)
N2	7(9)	1863(3)	2335(5)	C17	2846(17)	947(7)	3423(8)
C1	2258(6)	2685(2)	1133(4)	C18	6950(20)	–477(7)	2425(12)
C2	3931(6)	2858(2)	1265(4)	C19	4051(15)	1107(6)	191(8)
C3	4338(6)	3450(2)	1077(4)	C21	–213(13)	1692(5)	–652(7)
C4	3072(6)	3869(2)	757(4)	C22	–1115(16)	1465(7)	–1484(8)
C5	1399(6)	3696(2)	625(4)	C23	–1804(15)	917(7)	–1483(10)
C6	992(6)	3104(2)	813(4)	C24	–1602(16)	609(5)	–686(11)
C7	5355(11)	2430(5)	1649(9)	C25	–686(13)	848(5)	134(7)
C8	3495(18)	4515(6)	474(11)	C26	–1179(11)	1480(5)	2426(7)
C9	–821(12)	2968(5)	701(8)	C27	–2060(12)	1525(5)	3130(8)
C11	3386(6)	1018(2)	1789(4)	C28	–1695(13)	1963(6)	3771(7)
C12	3639(6)	738(2)	2661(4)	C29	–500(15)	2376(5)	3674(8)
C13	4776(6)	263(2)	2875(4)	C30	344(14)	2320(5)	2959(8)
C14	5660(6)	67(2)	2217(4)				

Å, H33–Fe1–H67 = 163°, H27–Fe2–H73 = 165°. The direction of the Fe···H interactions are approximately perpendicular to the respective coordination planes; the dihedral angles which they form with the normal to the coordination planes range from 17° to 19°. A significant parameter which should also be related is the distance of the iron atoms from the center of C–H bonds: Fe1···H33–C33, 2.55 Å; Fe1···H67–C67, 2.65 Å; Fe2···H27–C27, 2.62 Å; Fe2···H73–C73, 2.63 Å. Such short distances may be viewed as three-center four-electron interactions,[8] or they may arise simply from rigid or sterically constrained ligands.[9]

A monomeric form of iron–mesityl can be obtained from the reaction of **1** with pyridine in toluene, as reported in reaction 2.

$$\underset{\mathbf{1}}{Fe_2Mes_4} \xrightarrow[\text{toluene}]{Py} \underset{\mathbf{3}}{2\ Py_2FeMes_2} \qquad (2)$$

Although the monomeric form is a good source of Fe(II) in aprotic solvents, the chemistry associated with the reactivity of its iron–aryl functionality is not significantly different from that found for **1**. Complex **3** has the structure shown in Figure 2. It consists of discrete monomeric units where two mesityl ligands coordinate to iron through σ bonds (Figure 2). Tetrahedral coordination is completed by two pyridine molecules (Table 8). The Fe–C carbon bonds are significantly longer than those found for terminal mesityls in complex **1**, as a consequence of the increased coordination number of the metal [Fe–C_{av}, 2.020(5) Å, **1**; 2.148(5) Å; **3**]. The C1···C6 mesityl ring forms a dihedral angle of 68.4(2)° with respect to the C11···C16 ring. It is nearly perpendicular with respect to the N1–Fe–N2 plane [dihedral angle 87.7(2)°] bisecting the N1–Fe–N2 angle [distance of N1

(8) Anklin, C. G.; Pregosin, P. S. *Magn. Reson. Chem.* **1985**, *23*, 671. Brammer, L.; Charnock, J. M.; Goggin, P. L.; Goodfellow, R. J.; Orpen, A. G.; Koetzle, T. F. *J. Chem. Soc., Dalton Trans.* **1991**, 1789. Wehman-Ooyevaar, I. C. M.; Grove, D. M.; Kooijman, H.; van der Sluis, P.; Speck, A. L.; van Koten, G. *J. Am. Chem. Soc.* **1992**, *114*, 9916.

(9) Sunquist, W. I.; Bancroft, D. P.; Lippard, S. J. *J. Am. Chem. Soc.* **1990**, *112*, 1590.

Table 4. Fractional Atomic Coordinates (×10⁴) for Complex **4**

atom	x/a	y/b	z/c	atom	x/a	y/b	z/c
Fe	−2042.4(3)	2802.9(15)	2095.1(3)	C21	−499(2)	1523(3)	3250(2)
N1	−1894(2)	4195(3)	1419(2)	C22	−219(3)	496(4)	2916(2)
N2	−2003(2)	1622(3)	3439(2)	C23	685(3)	313(4)	3042(2)
C1	−436(2)	4869(3)	2372(2)	C24	1320(3)	1120(5)	3481(3)
C2	355(2)	4453(4)	2261(2)	C25	1038(3)	2114(4)	3812(3)
C3	1131(2)	5125(4)	2591(2)	C26	146(2)	2346(4)	3707(2)
C4	1147(3)	6192(4)	3027(2)	C27	−884(3)	−401(4)	2416(3)
C5	363(3)	6553(4)	3146(2)	C28	2302(3)	939(6)	3575(3)
C6	−425(2)	5902(3)	2839(2)	C29	−96(3)	3471(4)	4080(2)
C7	387(3)	3277(4)	1825(3)	C30	−1471(2)	1845(3)	3044(2)
C8	1984(3)	6934(5)	3348(3)	C31	−1827(2)	874(4)	4171(2)
C9	−1239(3)	6269(4)	3031(3)	C32	−1009(3)	1292(4)	4838(2)
C10	−1264(2)	4137(3)	2055(2)	C33	−1709(3)	−486(4)	3992(3)
C11	−2045(3)	5007(4)	715(2)	C34	−2654(3)	1012(5)	4439(2)
C12	−1956(3)	6361(4)	958(3)	C1S	489(6)	−2243(8)	1085(6)
C13	−2987(3)	4747(5)	189(3)	C2S	128(11)	−1578(18)	393(11)
C14	−1364(3)	4678(5)	320(3)	C3S	168(12)	−412(17)	338(8)

Table 5. Fractional Atomic Coordinates (×10⁴) for Complex **6**[a]

atom	x/a	y/b	z/c	atom	x/a	y/b	z/c
Fe	3796.6(6)	2325.5(5)	1524.2(7)	N5	2340(3)	2117(3)	1011(4)
N1	6741(3)	2124(3)	3657(4)	N6	3362(3)	2754(2)	−260(4)
N2	5023(3)	1739(2)	2343(4)	C31	51(4)	2421(4)	−197(5)
N3	4633(3)	3248(2)	2803(4)	C32	−926(4)	2335(4)	−1257(6)
C1	7307(4)	1449(3)	3478(5)	C33	−1810(5)	2248(6)	−866(8)
C2	8293(4)	1457(4)	4558(5)	C34	−1822(6)	2948(7)	−55(8)
C3	8926(4)	784(4)	4425(6)	C35	−842(5)	3064(5)	1016(6)
C4	9140(4)	862(4)	3289(6)	C36	57(5)	3150(4)	605(6)
C5	8171(5)	895(4)	2199(6)	C37	1790(4)	2425(3)	−56(5)
C6	7520(4)	1565(4)	2349(5)	C38	1846(4)	1618(4)	1658(5)
C7	5797(4)	2196(3)	3107(5)	C39	1444(5)	792(4)	1027(6)
C8	5094(4)	851(3)	2205(5)	C40	927(6)	253(4)	1686(7)
C9	5156(4)	414(3)	3334(5)	C41	1623(7)	129(6)	2926(9)
C10	5188(5)	−520(4)	3196(6)	C42	2062(5)	936(6)	3595(6)
C11	4257(5)	−845(4)	2138(7)	C43	2555(4)	1515(5)	2924(5)
C12	4202(5)	−414(4)	1007(6)	C44	2404(4)	2729(3)	−778(5)
C13	4194(4)	511(3)	1149(5)	C45	4102(4)	3031(4)	−796(5)
C14	5518(4)	3038(3)	3414(5)	C46A	4919(12)	2419(11)	−450(16)
C15	4190(4)	4028(4)	3000(5)	C47A	3785(10)	3194(9)	−2152(13)
C16	4844(6)	4793(4)	3014(7)	C48A	4569(11)	3913(9)	−173(14)
C17	3225(5)	4095(4)	1976(6)	C46B	3912(13)	2463(11)	−1991(15)
C18	4021(6)	3983(5)	4164(7)	C47B	3988(16)	3905(13)	−1199(20)
C21	6331(2)	3485(2)	4423(3)	C48B	5153(13)	2819(11)	100(16)
C22	6410(2)	3341(2)	5587(3)	C51	1797(3)	2949(2)	−2017(3)
C23	7182(2)	3733(2)	6536(3)	C52	1537(3)	2345(2)	−2914(3)
C24	7876(2)	4268(2)	6320(3)	C53	988(3)	2538(2)	−4086(3)
C25	7796(2)	4412(2)	5157(3)	C54	698(3)	3334(2)	−4361(3)
C26	7024(2)	4020(2)	4208(3)	C55	958(3)	3937(2)	−3464(3)
C27	5745(5)	2689(4)	5839(5)	C56	1507(3)	3744(2)	−2291(3)
C28	8731(5)	4695(5)	7357(6)	C57	1765(6)	1459(4)	−2636(6)
C29	7028(5)	4123(4)	2967(6)	C58	120(7)	3544(5)	−5648(7)
N4	853(3)	2538(3)	−639(4)	C59	1677(5)	4388(4)	−1335(5)

[a] The site occupation factors of C46–C48 are 0.55 and 0.45 for A and B positions, respectively.

and N2 from the plane through C1···C6 being 1.723(7) and −1.622(7) Å].

We explored the reactivity of **1** toward substrates which insert into the iron–carbon functionality. The reaction of **1** with Bu^{t}NC led to the insertion of the isocyanide into all of the iron–carbon bonds forming the homoleptic dinuclear iminoacyl **4**.

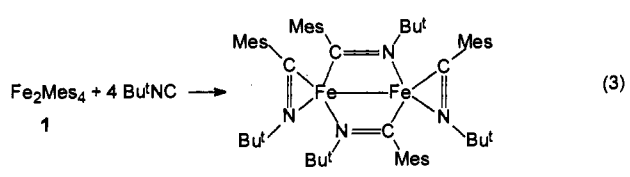

[{η²-C(Mes)=NBu^t}$_2$Fe$_2$(μ-C(Mes)=NBu^t)$_2$], **4**

Reaction 3 was carried out at 0 °C in THF, and complex **4** forms regardless of the Fe/RNC stoichiometry. The black crystalline solid **4** showed a significant increase in thermal stability *vs* **1**. The only spectroscopically significant features of **4** are the iminoacyl bands in the IR spectrum centered at 1600 cm^{-1}. According to the X-ray structure shown in Figure 3, the dimer **4**, having a C_2 crystallographic symmetry, contain both terminal η^2-C,N and bridging μ_2-C,N iminoacyls. The six-membered bimetallic ring has a boat conformation, and the dihedral angle between the Fe,C30,N2,Fe′ and Fe,C30′,N2′,Fe′ mean planes is 104.0(1)°. The structural parameters are only slightly different for the η^2- and the μ_2-iminoacyl moieties. The iron atom is displaced by 0.083(1) Å from the C1,C10,N1 plane involving the η^2-bonded atoms and by 0.112(1) Å from the plane through the C21,C30,N2 plane involving plane the bridging iminoacyl. The group of atoms C10,N1,C30,N2′ defines a plane (coordination plane, maximum deviation 0.026(3) Å for C10) from which iron is displaced by 0.160(1) Å in the direction of Fe′. The direction of the Fe···Fe′ interaction forms a dihedral angle of 32.8(6)° with respect to the normal of the coordination plane. The C1···C6 aromatic ring is twisted by 85.6(1)° with respect to the

Table 6. Fractional Atomic Coordinates ($\times 10^4$) for Complex **7**

atom	x/a	y/b	z/c	atom	x/a	y/b	z/c
Fe	436.8(9)	894.7(7)	393.1(9)	C23	−4088(3)	3968(2)	−1792(4)
N1	24(5)	1745(5)	2261(6)	C24	−3445(3)	4650(2)	−1097(4)
N2	−1078(4)	709(4)	−564(5)	C25	−2342(3)	4204(2)	−434(4)
C1	−96(4)	2680(4)	4667(4)	C26	−1881(3)	3076(2)	−468(4)
C2	−617(4)	2347(4)	5384(4)	C31	−2844(3)	531(3)	−1985(3)
C3	−654(4)	2840(4)	6708(4)	C32	−2724(3)	35(3)	−3294(3)
C4	−170(4)	3666(4)	7315(4)	C33	−3355(3)	−649(3)	−4026(3)
C5	351(4)	3999(4)	6598(4)	C34	−4106(3)	−838(3)	−3450(3)
C6	388(4)	3506(4)	5274(4)	C35	−4225(3)	−343(3)	−2141(3)
C7	−50(6)	2172(6)	3332(7)	C36	−3595(3)	341(3)	−1408(3)
C11	1362(3)	1555(3)	−330(4)	C37	−1996(6)	301(6)	−3954(6)
C12	1637(3)	1021(3)	−1586(4)	C38	−4749(9)	−1621(8)	−4214(11)
C13	2320(3)	1341(3)	−2107(4)	C39	−3793(6)	906(7)	−4(7)
C14	2730(3)	2196(3)	−1374(4)	C27	−2063(5)	1192(5)	−1174(6)
C15	2456(3)	2731(3)	−118(4)	C41	7149(6)	5049(5)	4390(11)
C16	1772(3)	2410(3)	404(4)	C42	7226(6)	4520(5)	3080(11)
C17	1205(8)	103(6)	−2426(7)	C43	6861(6)	3610(5)	2520(11)
C18	3455(7)	2564(7)	−1980(9)	C44	6420(6)	3230(5)	3270(11)
C19	1527(8)	3004(7)	1748(8)	C45	6343(6)	3759(5)	4580(11)
C21	−2524(3)	2394(2)	−1163(4)	C46	6708(6)	4668(5)	5140(11)
C22	−3628(3)	2840(2)	−1826(4)				

Table 7. Selected Bond Distances (Å) and Angles (deg) for Complex **2**

Fe1–Fe2	2.666(3)	Fe2–C21	2.188(8)
Fe1–C1	2.083(9)	Fe2–C41	2.104(9)
Fe1–C21	2.159(9)	Fe2–C61	2.176(9)
Fe1–C61	2.169(8)		
C21–Fe1–C61	104.9(3)	Fe1–C1–C2	120.4(6)
C1–Fe1–C61	126.5(3)	Fe1–C21–Fe2	75.6(3)
C1–Fe1–C21	128.5(3)	Fe2–C21–C26	125.4(6)
Fe2–Fe1–C61	52.3(2)	Fe2–C21–C22	102.6(6)
Fe2–Fe1–C21	52.7(3)	Fe1–C21–C26	100.9(6)
Fe2–Fe1–C1	178.1(3)	Fe1–C21–C22	126.5(7)
Fe1–Fe2–C61	52.0(2)	Fe2–C41–C46	120.0(6)
Fe1–Fe2–C41	178.1(3)	Fe2–C41–C42	119.8(6)
Fe1–Fe2–C21	51.7(2)	Fe1–C61–Fe2	75.7(3)
C41–Fe2–C61	129.5(3)	Fe2–C61–C66	101.7(6)
C21–Fe2–C61	103.7(3)	Fe2–C61–C62	127.1(6)
C21–Fe2–C41	126.7(3)	Fe1–C61–C66	124.2(6)
Fe1–C1–C6	119.5(6)	Fe1–C61–C62	102.1(6)

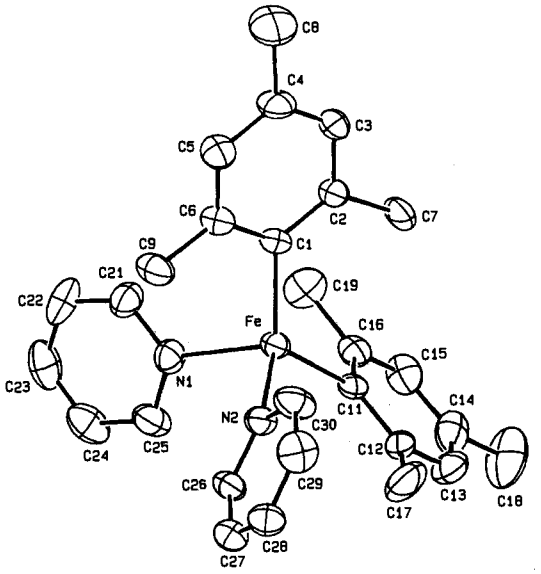

Figure 2. ORTEP drawing for complex **3** (30% probability ellipsoids).

coordination plane. The Fe,C30,N2,Fe′ ring is approximately planar [max deviation 0.121(3) Å for C30]. The mean plane through these atoms forms dihedral angles of 68.9(1)° and 84.8(1)° with the coordination plane and the C21···C26 ring, respectively. The distortion from the regular sp^2 geometry around

Table 8. Selected Bond Distances (Å) and Angles (deg) for Complex **3**

Fe–N1	2.179(7)	N1–C21	1.309(13)
Fe–N2	2.169(8)	N1–C25	1.368(14)
Fe–C2	2.156(5)	N2–C26	1.318(13)
Fe–C11	2.141(5)	N2–C30	1.352(13)
C1–Fe–C11	128.8(2)	C21–N1–C25	116.1(8)
N2–Fe–C11	112.0(2)	Fe–N2–C30	116.5(7)
N2–Fe–C1	101.6(2)	Fe–N2–C26	125.5(6)
N1–Fe–C11	102.7(3)	C26–N2–C30	117.4(9)
N1–Fe–C1	107.8(3)	Fe–C1–C6	121.4(4)
N1–Fe–N2	100.7(3)	Fe–C1–C2	118.5(3)
Fe–N1–C25	121.3(6)	Fe–C11–C16	116.9(4)
Fe–N1–C21	121.5(7)	Fe–C11–C12	123.1(4)

C10 and N2, and in particular the narrowing of the Fe–C30–N2 [112.5(3)°] and Fe′–N2–C30 [98.1(2)°] bond angles, are consistent with a metal–metal bond. This is supported by a rather short Fe–Fe distance [2.371(4) Å],[10a] the shortest Fe–Fe distance being very recently reported.[10b] The other structural parameters which should be considered are the Fe–C bond distances, which are much shorter than those of **1**, **2**, and **7**. This can be in agreement with considerable carbenoid character for the iminoacyl carbon,[11] additionally supported by rather short Fe–N [Fe–N1, 2.007(4) Å; Fe–N2′, 1.987(3) Å] and C–N [C10–N1, 1.265(4) Å; C30–N2, 1.292(6) Å] bond distances (Table 9).

A very short Fe–Fe distance, while in agreement with the existence of a metal–metal bond, does not unequivocally prove its presence.[12] The magnetic properties of the dimer **4** can clearly address the problem, showing the unquestioned presence of the iron–iron bond (*vide infra*). The formation of an iminoacyl from the migratory insertion[11,13] of an isocyanide into an alkyl is well known.[14] The formation of an iron–iminoacyl, either from a migratory insertion reaction[15] or from other reactions,[16] has a number of precedents. The resulting η^2-bonding mode is quite common, while the bridging bonding mode μ_2-C,N is much more rare.[16d] In addition, the iminoacyl functionality is usually found on a metal surrounded by ancillary ligands. Homoleptic iminoacyls have some significant examples in early transition metal chemistry,[11,14] but they are very rare or almost unknown for middle and late transition metals.

(10) (a) Fehlhammer, W. P.; Stolzenberg, H. Dinuclear Iron Compounds with Hydrogen Ligands. In *Comprehensive Organometallic Chemistry*; Wilkinson, G.; Stone, F. G. A., Abel, E. W., Eds.; Pergamon: Oxford, U.K., 1982; Vol. 4, Chapter 31.4. (b) Cotton, F. A.; Daniels, L. M.; Falvello, L. R.; Murillo, C. A. *Inorg. Chim. Acta* **1994**, *219*, 7.

(11) Durfee, L. D.; Rothwell, I. P. *Chem. Rev.* **1988**, *88*, 1059.

(12) Cotton, F. A.; Walton, R. A. *Multiple Bonds between Metal Atoms*; Clarendon: Oxford, U.K., 1993.

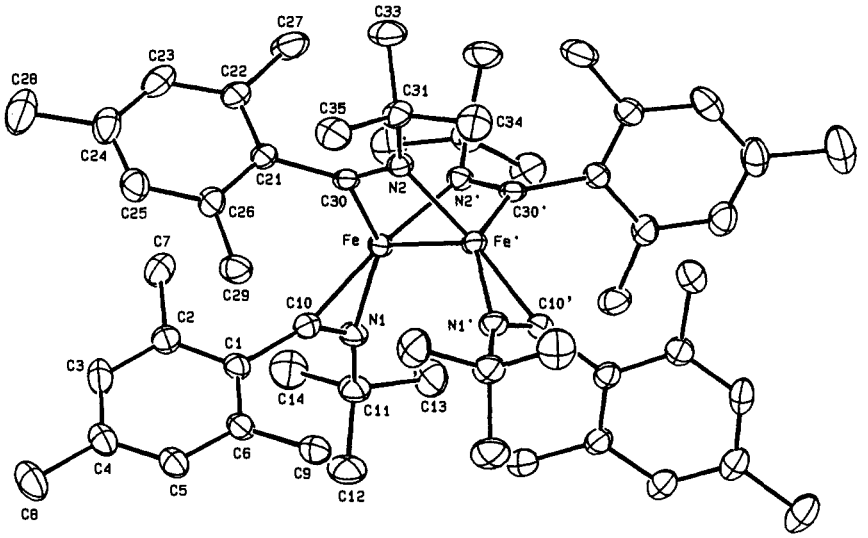

Figure 3. ORTEP drawing for complex **4** (30% probability ellipsoids). Prime denotes a transformation of $-0.5 - x, y, 0.5 - z$.

Table 9. Selected Bond Distances (Å) and Angles (deg) for Complex **4**[a]

Fe···Fe'	2.371(4)	N1–C11	1.507(5)
Fe–N1	2.007(4)	N2–C30	1.292(6)
Fe–N2'	1.987(3)	N2–C31	1.504(5)
Fe–C10	1.921(3)	C1–C10	1.487(4)
Fe–C30	1.968(3)	C21–C30	1.509(4)
N1–C10	1.265(4)		
C10–Fe–C30	108.0(1)	C10–N1–C11	131.9(3)
N1–Fe–C30	145.2(1)	C30–N2–C31	128.2(3)
N1–Fe–C10	37.5(1)	N1–C10–C1	132.2(3)
N2'–Fe–C30	98.8(1)	Fe–C10–C1	152.8(3)
N2'–Fe–C10	150.4(1)	Fe–C10–N1	74.9(2)
N2'–Fe–N1	114.1(1)	N2–C30–C21	128.1(3)
C30–N2–Fe'	98.1(2)	Fe–C30–C21	119.3(2)
Fe'–Fe–N1	126.3(1)	Fe–C30–N2	112.5(3)
Fe'–Fe–N2	77.2(1)	N2–C31–C34	106.6(3)
Fe'–Fe–C30	70.3(1)	N2–C31–C33	109.5(3)
Fe–N1–C11	160.1(3)	N2–C31–C32	114.1(3)
Fe–N1–C10	67.6(2)		

[a] Prime denotes a transformation of $-0.5 - x, y, 0.5 - z$.

Metal–acyls and metal–iminoacyls are fundamental organometallic functionalities.[11,13] While much attention has been devoted to their formation by the migratory insertion of carbon monoxide and isocyanides into the metal–carbon bond,[9–11,13] their chemistry has been little explored, except for early transition metal η^2-acyl complexes. They undergo reductive elimination reactions,[17] show general carbenoid behavior,[18,19] and are transformable to metal enolates or metal ketenes.[20] Their apparently low reactivity contrasts with the usual assumption that metal–acyls or metal–iminoacyls are intermediates in metal-mediated catalytic processes. Therefore there are some questions which need to be addressed for understanding the intermediacy of such species in catalytic processes. Among them: can a metal–acyl (or –iminoacyl) insert other functionalities?[21]

The Fe–C bonds present in **4** do not react further with isocyanides, but they are reactive with other inserting substrates.

(13) For a general review on migratory insertion reaction, see: (a) Tatsumi, K.; Nakamura, A.; Hofmann, P.; Stauffert, P.; Hoffmann, R. *J. Am. Chem. Soc.* **1985**, *107*, 4440. (b) Hofmann, P.; Stauffert, P.; Tatsumi, K.; Nakamura, A.; Hoffmann, R. *Organometallics* **1985**, *4*, 404 (bonding and many references). (c) Rusik, C. A.; Tonker, T. L.; Templeton, J. L. *J. Am. Chem. Soc.* **1986**, *108*, 4652. (d) Arnold, J.; Tilley, T. D. *J. Am. Chem. Soc.* **1986**, *108*, 5355. Curtis, M. D.; Shiu, K.-B.; Butler, W. M. *J. Am. Chem. Soc.* **1986**, *108*, 1550. Moloy, K. G.; Fagan, P. J.; Manriquez, J. M.; Marks, T. J. *J. Am. Chem. Soc.* **1986**, *108*, 56. Martin, B. D.; Matchett, S. A.; Norton, J. R.; Anderson, O. P. *J. Am. Chem. Soc.* **1985**, *107*, 7952. Collmann, J. P.; Hegedus, L. S.; Norton, J. R.; Finke, R. G. *Principles and Applications of Organotransition Metal Chemistry*; University Science Books: Mill Valley, CA, 1987. Anderson, G. K.; Cross, R. J. *Acc. Chem. Res.* **1984**, *17*, 67. Braterman, P. S. In *Reactions of Coordinated Ligands*; Braterman, P. S., Ed.: Plenum: New York, 1986; Chapter 6. Ziegler, T.; Versluis, L.; Tschinke, V. *J. Am. Chem. Soc.* **1986**, *108*, 612. Erker, G. *Acc. Chem. Res.* **1984**, *17*, 103.

(14) Singleton, E.; Ossthnizen, H. E. *Adv. Organomet. Chem.* **1983**, *22*, 209. Otsuka, S.; Nakamura, A.; Yoshida, T.; Naruto, M.; Ataba, K. *J. Am. Chem. Soc.* **1973**, *95*, 3180. Yamamoto, Y.; Yamazaki, H. *Inorg. Chem.* **1974**, *13*, 438. Aoki, K.; Yamamoto, Y. *Inorg. Chem.* **1976**, *15*, 48. Bellachioma, G.; Cardaci, G.; Zanazzi, P. *Inorg. Chem.* **1987**, *26*, 84. Maitlis, P. M.; Espinet, P.; Russell, M. J. H. In *Comprehensive Organometallic Chemistry*; Wilkinson, G., Stone, F. G. A., Abel, E. W., Eds.; Pergamon: London, 1982; Vol. 8, Chapter 38.4. Crociani, B. In *Reactions of Coordinated Ligands*; Braterman, P. S., Ed.; Plenum: New York, 1986; Chapter 9.

(15) (a) Bellachioma, G.; Cardaci, G.; Macchioni, A.; Reichenbach, G. *Inorg. Chem.* **1992**, *32*, 63 and references therein. (b) Cardaci, G.; Bellachioma, G.; Zanazzi, P. *Polyhedron* **1983**, *2*, 967.

(16) (a) Fehlhammer, W. P.; Hirschmann, P.; Mayr, A. *J. Organometal. Chem.* **1982**, *224*, 153. (b) Brunner, H.; Kerkien, G.; Wachter, J. *J. Organometal. Chem.* **1982**, *224*, 295. (c) Adams, R. D.; Chodosh, D. F.; Golembeski, N. M.; Weissman, E. C. *J. Organometal. Chem.* **1979**, *172*, 251. (d) Seyferth, D.; Hoke, J. B. *Organometallics* **1988**, *7*, 524 and references therein.

(17) Waymouth, R. M.; Grubbs, R. H. *Organometallics* **1988**, *7*, 1631. Erker, G.; Dorf, U.; Czisch, P.; Petersen, J. L. *Organometallics* **1986**, *5*, 668. Rosenfeldt, F.; Erker, G. *Tetrahedron Lett.* **1980**, *21*, 1637. Berno, P.; Stella, S.; Floriani, C.; Chiesi-Villa, A.; Guastini, C. *J. Chem. Soc., Dalton Trans.* **1990**, 2669.

(18) Manriquez, J. M.; McAlister, D. R.; Sanner, R. D.; Bercaw, J. E. *J. Am. Chem. Soc.* **1978**, *100*, 2716; **1976**, *98*, 6733. McCleverty, J. A.; Wilkinson, G. *J. Chem. Soc.* **1963**, 4096. Tatsumi, K.; Nakamura, A.; Hofmann, P.; Hoffmann, R.; Moloy, K. G.; Marks, T. J. *J. Am. Chem. Soc.* **1986**, *108*, 4467. Erker, G.; Kropp, K.; Kruger, C.; Chiang, A.-P. *Chem. Ber.* **1982**, *115*, 2447. Petersen, J. L.; Egan, J. W., Jr. *Organometallics* **1987**, *6*, 2007.

(19) Chamberlain, L. R.; Durfee, L. D.; Fanwick, P. E.; Kobriger, L. M.; Latesky, S. L.; McMullen, A. K.; Steffey, B. D.; Rothwell, I. P.; Folting, K.; Huffman, J. C. *J. Am. Chem. Soc.* **1987**, *109*, 6068. Chamberlain, L. R.; Rothwell, I. P.; Huffman, J. C. *J. Chem. Soc., Chem. Commun.* **1986**, 1203. Chamberlain, L. R.; Steffey, B. D.; Rothwell, I. P.; Huffman, J. C. *Polyhedron* **1989**, *8*, 341. McMullen, A. K.; Rothwell, I. P.; Huffman, J. C. *J. Am. Chem. Soc.* **1985**, *107*, 1072. Durfee, L. D.; McMullen, A. K.; Rothwell, I. P. *J. Am. Chem. Soc.* **1988**, *110*, 1463.

(20) Waymouth, R. M.; Santarsiero, B. D.; Coots, R. J.; Bronikowski, M. J.; Grubbs, R. H. *J. Am. Chem. Soc.* **1986**, *108*, 1427. Waymouth, R. M.; Clauser, K. R.; Grubbs, R. H. *J. Am. Chem. Soc.* **1986**, *108*, 6385. Waymouth, R. M.; Santarsiero, B. D.; Grubbs, R. H. *J. Am. Chem. Soc.* **1984**, *106*, 4050. Ho, S. C. H.; Straus, D. A.; Armantrout, J.; Schaefer, W. P.; Grubbs, R. H. *J. Am. Chem. Soc.* **1984**, *106*, 2210. Moore, E. J.; Straus, D. A.; Armantrout, J.; Santarsiero, B. D.; Grubbs, R. H.; Bercaw, J. E. *J. Am. Chem. Soc.* **1983**, *105*, 2068. Stille, J. R.; Grubbs, R. H. *J. Am. Chem. Soc.* **1983**, *105*, 1664.

(21) A limited number of cases have been reported in case of lanthanides and actinides: Andersen, R. A. *Inorg. Chem.* **1979**, *18*, 2928. Fagan, P. J.; Manriquez, J. M.; Marks, T. J.; Day, V. W.; Vollmer, S. H.; Day, S. C. *J. Am. Chem. Soc.* **1980**, *102*, 5393. Lappert, M. T.; Raston, C. L.; Engelhardt, L. M.; White, A. H. *J. Chem. Soc., Chem. Commun.* **1985**, *521*. Campion, B. K.; Falk, J.; Tilley, T. D. *J. Am. Chem. Soc.* **1987**, *109*, 2049. Arnold, J.; Tilley, T. D. *J. Am. Chem. Soc.* **1985**, *107*, 6049.

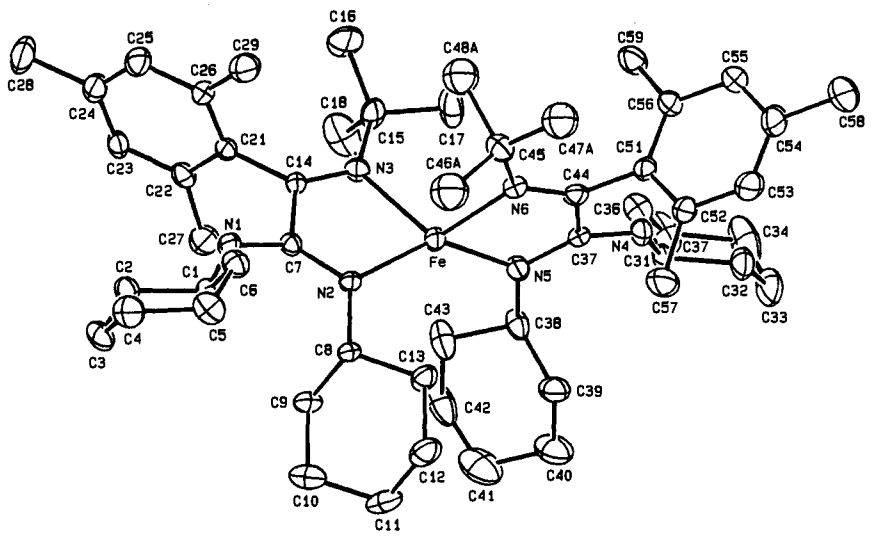

Figure 4. ORTEP drawing for complex **6** (30% probability ellipsoids). Only the A position is given for the disordered C46–C48 atoms.

This permits a rather interesting selective sequence for the insertion into an iron–aryl carbon bond.

When the reaction of **4** with carbon dioxide is carried out in THF at 0 °C, and then at room temperature, complex **5** is formed as a yellow crystalline solid, when recrystallized from Et_2O.

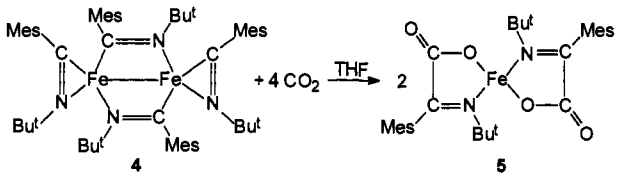

The insertion of carbon dioxide occurs on each iron–carbon bond and a mononuclear species is generated where iron is surrounded by two bidentate anions formally derived from an α-imino acid. The migratory insertion aptitude of an iminoacyl is quite rare[11,19] and opens up the possibility of a sequential insertion of different functional groups on a metal–carbon bond. The iron–carbon bond in **4** does not have migratory aptitude with poorly polarized molecules like carbon monoxide, isocyanides, nitriles, *etc.*, but it maintains considerable reactivity with strong electrophiles like CO_2 and similar cumulenes. A number of reports deal with the insertion of CO_2 into metal–alkyl or metal–aryl bonds,[22] but very rarely does this occur on metal–α-functionalized alkyls or aryls.

The proposed structure of **5**, apart from the analytical and spectroscopic data reported in the experimental section, is based on its magnetic properties, which are typical of a monomeric high-spin d^6 complex, and on its very close relationship with the structure of **6** (determined with an X-ray analysis). When **4** was treated with CyN=C=NCy in toluene at −30 °C, and then at room temperature, **6** formed as a red crystalline solid.

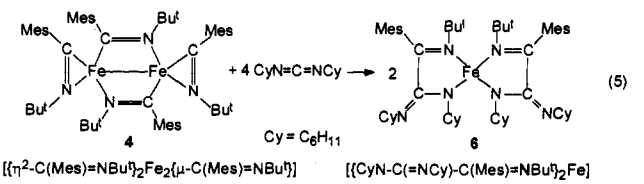

(5)

(22) (a) Behr, A. *Carbon Dioxide Activation by Metal Complexes*; VCH: Weinheim, FGR: 1988. (b) Darensbourg, D.; Kudaroski, R. A. *Adv. Organometal. Chem.* **1983**, *22*, 129. (c) Behr, A. *Angew. Chem., Int. Ed. Engl.* **1988**, *27*, 661. (d) Braunstein, P.; Matt, D.; Nobel, D. *Chem. Rev.* **1988**, *88*, 747. (e) Walther, D. *Coord. Chem. Rev.* **1987**, *79*, 135.

Table 10. Selected Bond Distances (Å) and Angles (deg) for Complex **6**

Fe–N2	1.987(4)	N4–C31	1.452(9)
Fe–N3	2.130(4)	N4–C37	1.301(6)
Fe–N5	1.974(4)	N5–C37	1.360(7)
Fe–N6	2.150(5)	N5–C38	1.467(9)
N1–C1	1.472(8)	N6–C44	1.291(7)
N1–C7	1.292(7)	N6–C45	1.497(9)
N2–C7	1.344(6)	C7–C14	1.539(8)
N2–C8	1.476(6)	C14–C21	1.499(5)
N3–C14	1.287(6)	C37–C44	1.529(10)
N3–C15	1.516(8)	C44–C51	1.490(6)
N5–Fe–N6	81.0(2)	C37–N5–C38	119.8(5)
N3–Fe–N6	111.9(1)	Fe–N6–C45	122.7(3)
N3–Fe–N5	123.8(2)	Fe–N6–C44	111.1(4)
N2–Fe–N6	124.2(2)	C44–N6–C45	126.2(5)
N2–Fe–N5	138.2(2)	N1–C7–N2	136.7(5)
N2–Fe–N3	80.6(2)	N2–C7–C14	113.7(5)
C1–N1–C7	125.5(5)	N1–C7–C14	109.5(5)
Fe–N2–C8	123.9(4)	N3–C14–C7	116.7(5)
Fe–N2–C7	115.6(3)	C7–C14–C21	113.7(4)
C7–N2–C8	120.3(5)	N3–C14–C21	129.6(4)
Fe–N3–C15	122.6(3)	N4–C37–N5	136.2(6)
Fe–N3–C14	112.0(3)	N5–C37–C44	114.0(5)
C14–N3–C15	125.3(5)	N4–C37–C44	109.7(5)
C31–N4–C37	126.4(5)	N6–C44–C37	117.3(5)
Fe–N5–C38	124.4(4)	C37–C44–C51	114.2(5)
Fe–N5–C37	115.6(4)	N6–C44–C51	128.5(5)

The structure of **6** is shown in Figure 4, with the iron having a tetrahedral coordination geometry. The metallacycles show an envelope conformation with iron 0.206(1) and 0.171(1) Å out of the N2,C7,C14,N3 and N5,C37,C44,N6 planes, respectively. The average planes of the two rings are nearly perpendicular to each other, the dihedral angle being 89.2(1)°. All the other structure parameters listed in Table 10 are in agreement with the bonding scheme shown for **6**.

Reaction 3 is a stepwise process, where the precoordination of the Bu^tNC to iron is, very probably, followed by the migration of the more reactive bridging mesityl to the isocyanide, and successively the terminal mesityl would migrate to a second precoordinated Bu^tNC molecule. The reaction of **1** with benzonitrile shed light on the stepwise mechanism of the insertion into the iron–aryl bond and allowed the isolation of a structural model for this general reaction. A single insertion was observed in the reaction of C_6H_5CN with **1**, regardless of the stoichiometric ratio.

The bridging mesityl shows a higher migratory aptitude than the terminal one, which does not migrate to the coordinated benzonitrile (see complex **7**). In addition, complex **7** should be

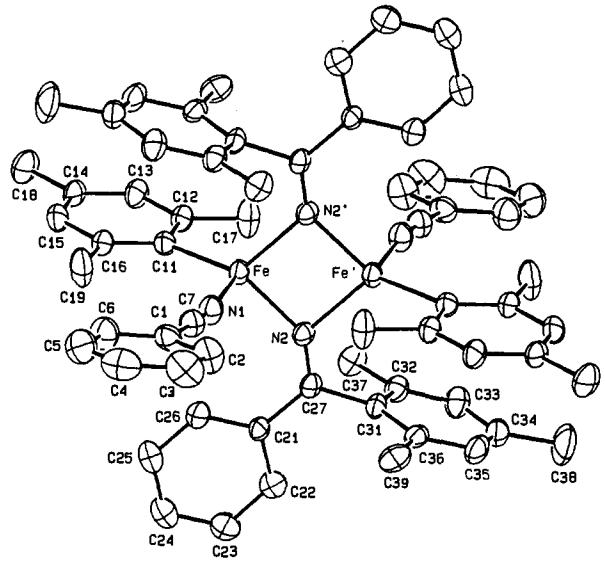

Figure 5. ORTEP drawing for complex **7** (30% probability ellipsoids). Prime denotes a transformation of $-x, -y, -z$.

Table 11. Selected Bond Distances (Å) and Angles (deg) for Complex **7**[a]

Fe–Fe'	2.859(2)	Fe–C11	2.118(5)
Fe–N1	2.088(6)	N1–C7	1.141(9)
Fe–N2	2.016(5)	N2–C27	1.281(7)
N1–Fe–C11	114.1(2)	Fe–C11–C16	124.0(3)
N1–Fe–N2	101.8(3)	Fe–C11–C12	115.9(3)
N2–Fe–C11	122.5(2)	N2–C27–C31	120.1(5)
N2'–Fe–C11	122.0(2)	N2–C27–C21	124.1(6)
N2'–Fe–N2	90.5(20	C42–C41–C46	120.0(8)
N2'–Fe–N1	101.4(3)	C41–C42–C43	120.0(9)
Fe–N1–C7	171.1(7)	C42–C43–C44	120.0(9)
Fe–N2–C27	143.5(5)	C43–C44–C45	120.0(7)
Fe–N2–Fe'	89.5(2)	C44–C45–C46	120.0(9)
N1–C7–C1	177.8(9)		

[a] Prime denotes a transformation of $-x, -y, -z$.

considered as a structural model for the precoordination of a substrate to the tricoordinate iron(II) in complex **1** in the preliminary stage preceding the aryl migration. The insertion of

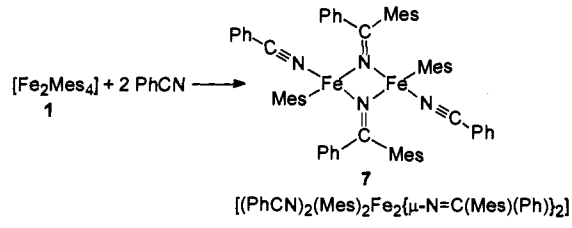

nitriles into a metal–carbon bond, although much more rare than the analogous reaction of isocyanides and carbon monoxide, has significant precedent in the literature.[23]

The magnetic properties of **7** will be discussed jointly with those of the other dimeric compounds (*vide infra*). Its ORTEP diagram is reported in Figure 5 with selected structural parameters in Table 11. The dimer has a center of gravity on a crystallographic center of symmetry at (0,0,0). The two irons are bonded to terminal Mes and PhCN groups and bridged by two diaryl imino groups. The Fe_2N_2 skeleton has a perfectly planar geometry. The dihedral angle between this plane and the plane containing the other two donor atoms around iron [Fe1,N2,-Fe1',N2'∠Fe1,C11,N1] is 89.9(2)°. The Fe–C11 bond distance [2.118(5) Å] is significantly longer than that in Fe_2Mes_4 [2.020-(5) Å] and close to those in **3**[3.141(5) Å] (Table 8). The Fe···Fe distance [2.859(2) Å] in **7** is much longer than that in complex **4**, even though the two iron(II) atoms are bridged by a single donor atom. The iron–iron distances in complexes **4** and **7** can hardly be compared with other iron–iron distances containing the metal normally in lower oxidation states, since the knowledge of iron(II)–iron(II) distances is very limited.[12]

The isolation of **7** may be a consequence of the much lower reactivity of nitriles *vs* isocyanides or carbon monoxide in insertion reactions. In addition, less polarized nitriles, like acetonitrile, do not react with **1**. More reactive inserting groups can, however, prompt **7** to undergo further insertion reactions into the terminal Mes groups. Such a reactivity was examined with three different substrates. The reaction with cyclohexylcarbodiimide and phenyl isocyanate led to insertion into the residual iron–mesityl bond and the formation of bidentate diamido and amido terminal ligands, preserving the dinuclear core while displacing the coordinated benzonitrile (reaction 7),

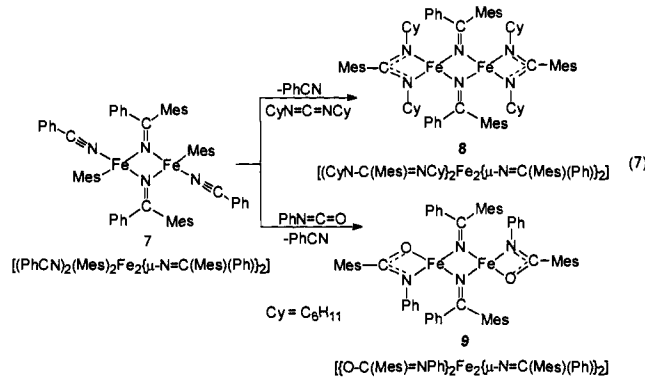

The analytical and spectroscopic results are in the Experimental Section and do not show any unusual characteristics. The proposed binuclear structure, which contains the diiron core intact, is mainly supported by the magnetic properties of **8** and **9**, which show very close similarities to those characteristic of the dinuclear unit in **7** (*vide infra*). The migratory aptitude of the terminal moiety in **7** has been observed also in reaction 8 when Bu^{t}NC is employed.

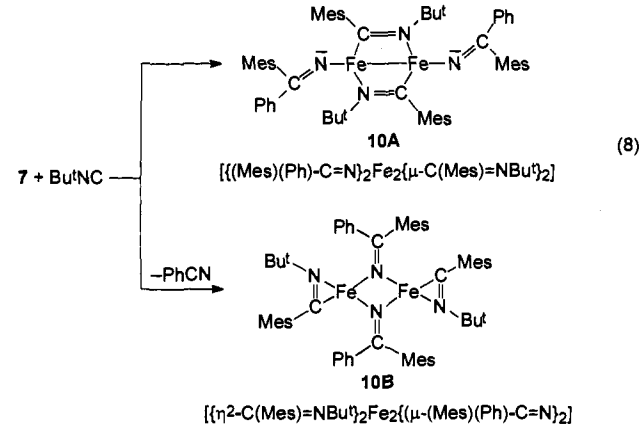

The residual mesityl group in **7** migrates very easily to Bu^{t}NC, and it displaces benzonitrile. The analytical and spectroscopic results are in agreement with both structures proposed for **10**. The analysis of the magnetic data, which will be examined in detail below, indicate that the diiron core of **7** is no longer preserved in **10**, which has magnetic properties very close to those of **4**. On this basis, we propose structure **A** for complex **10**. All the arguments supporting structure **A** are reported in the following section.

(23) Collman, J. P.; Hegedus, L. S.; Norton, J. R.; Finke, R. G. *Principles and Applications of Organotransition Metal Chemistry*; University Science Books: Mill Valley, CA, 1987.

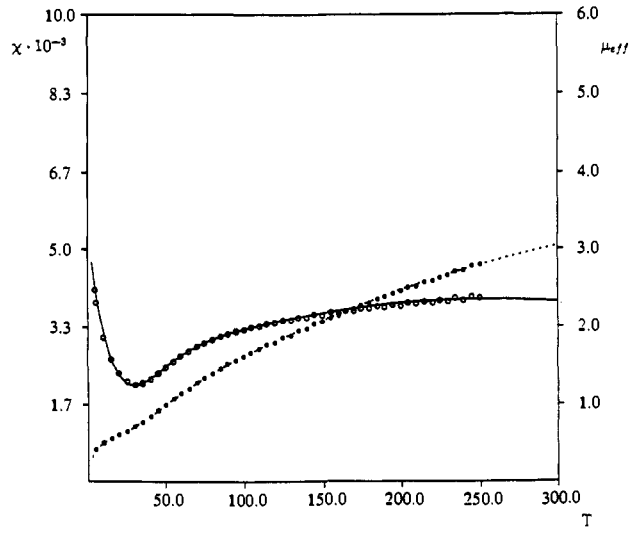

Figure 6. Magnetic susceptibility (O) and effective magnetic moment (●) per Fe of **7** as a function of the temperature. The solid and dashed lines are the best theoretical fits (see text) to the experimental data.

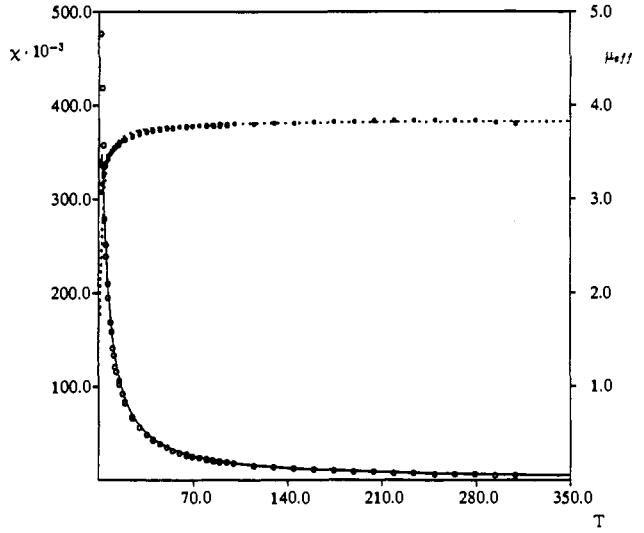

Figure 7. Magnetic susceptibility (O) and effective magnetic moment (●) per Fe of **4** as a function of the temperature. The solid and dashed lines are the best theoretical fits (see text) to the experimental data.

Magnetic Susceptibility Analysis. Magnetic susceptibilities data for complexes **1**, **4**, and **7**–**10** were collected in the temperature range 1.9–310 K and are displayed in Figures 6–11. For complexes **5** and **6**, the temperature dependence of magnetic susceptibility values are not reported as they show a constant value of μ_{eff} in a wide temperature range. The first analysis deals with complexes **1**, **4**, and **7**, which contain the three kinds of dinuclear skeletons present in all of our diiron complexes.

The magnetic moment *per* iron of **4** is essentially constant down to 10–20 K with a value of about 3.86 μ_B at 310 K while for complexes **1** and **7**, μ_{eff} decreases significantly with the temperature according to the presence of a relevant antiferromagnetic coupling. However, due to the short Fe–Fe distances observed in complexes **1**, **4**, and **7** [2.614(1) Å, **1**; 2.371(4) Å, **4**; 2.859(2) Å, **7**], we should consider how the metal–metal bonding can affect the magnetic coupling. In an attempt to fit the magnetic data, we used the simple[24] Heisenberg spin Hamiltonian (eq 9) considering a pair of exchange coupled ions with $S_1 = S_2 = 2$.

$$H_{ex} = -2J\hat{S}_1\hat{S}_2 \qquad (9)$$

(24) O'Connor, C. J. *Progr. Inorg. Chem.* **1982**, *29*, 203.

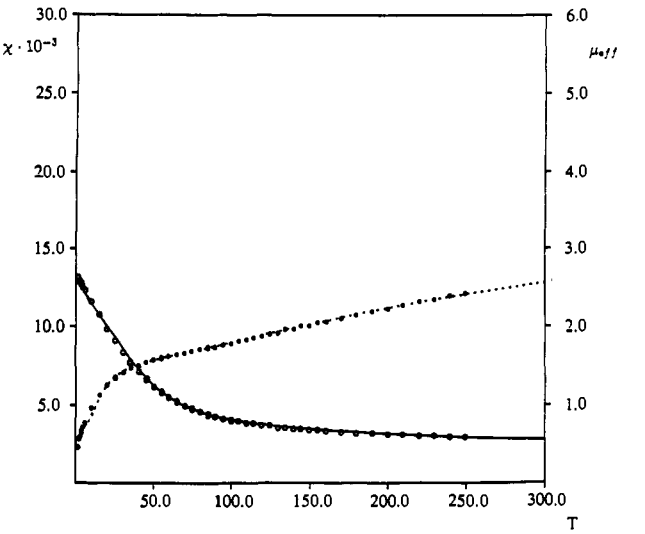

Figure 8. Magnetic susceptibility (O) and effective magnetic moment (●) per Fe of **1** as a function of the temperature. The solid and dashed lines are the best theoretical fits (see text) to the experimental data.

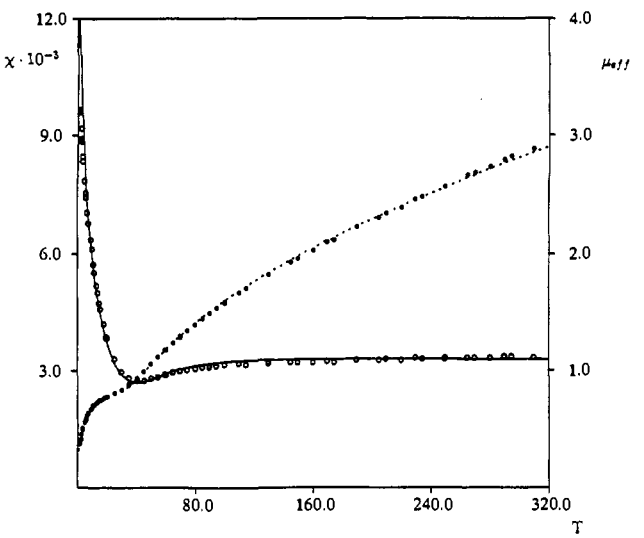

Figure 9. Magnetic susceptibility (O) and effective magnetic moment (●) per Fe of **8** as a function of the temperature. The solid and dashed lines are the best theoretical fits (see text) to the experimental data.

The presence of a small Curie tail in the magnetic susceptibility data at low temperature for complexes **1** and **7** requires a correction for a small amount of monomeric Fe(II) impurities which we assumed to obey Curie–Weiss law. Therefore the following equation is used for the total susceptibility, χ,

$$\chi = \frac{1}{2}(1 - x)\chi_{dim} + x\frac{Ng^2\mu_B{}^2S(S + 1)}{3K(T - \theta)} \qquad (10)$$

where S and g are the spin and the g factor of the impurity (assumed to be the same of the Fe(II) ion in the dimer), θ is its Weiss constant (which can be relevant due to large zero-field splitting usually observed for Fe(II) compounds), and x is the monomeric impurity fraction.

Magnetic data of complex **7** (Figure 6) have been analyzed, and their best fit has been obtained for $g = 2.34$, $J = -63.7$ cm^{-1}, $x = 1.9\%$, and $\theta = -15.3$ K. Such results support a strong antiferromagnetic coupling between the two iron(II) centers.

The analogous fit for **4** (Figure 7) gave $g = 1.56$ and $J = -0.4$ cm^{-1} with x being negligible. Such a g value, however, is exceedingly low for a Fe(II) ion, which usually show g values higher than 2.0 due to relevant orbital contribution. The μ_{eff} =

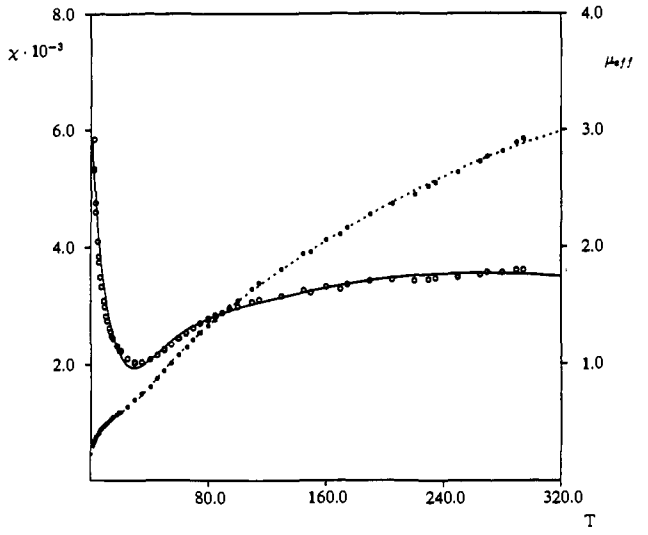

Figure 10. Magnetic susceptibility (O) and effective magnetic moment (●) per Fe of 9 as a function of the temperature. The solid and dashed lines are the best theoretical fits (see text) to the experimental data.

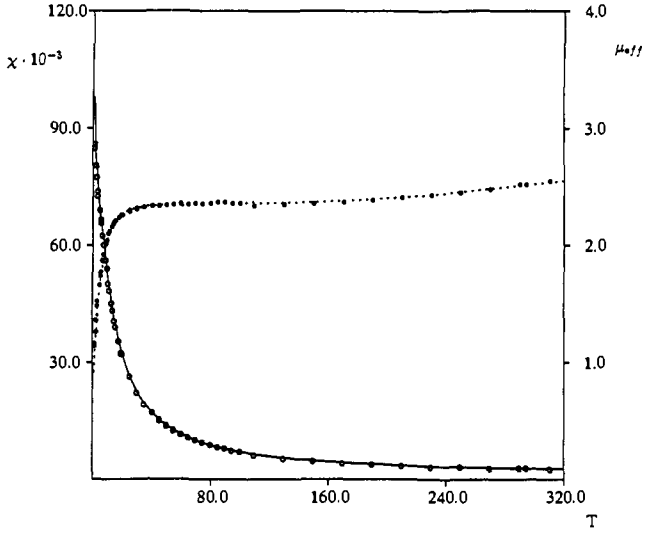

Figure 11. Magnetic susceptibility (O) and effective magnetic moment (●) per Fe of **10** as a function of the temperature. The solid and dashed lines are the best theoretical fits (see text) to the experimental data.

3.86 μ_B at 310 K corresponding to three unpaired electrons suggested the trial of a new fit using the susceptibility equation for two coupled ions with $S_1 = S_2 = {}^3/_2$. The more reasonable values of $g = 1.98$ and $J = -0.45$ cm^{-1} have been obtained. This result is in agreement with a Fe–Fe single bond, supported by the short Fe–Fe distance of 2.371(4) Å, which implies the strong coupling of one of the four unpaired electrons per iron atom. The J value indicates a very small antiferromagnetic coupling between the two effective $S = {}^3/_2$ centers through the bridging μ_2-iminoacyls. The low value of the coupling constant also implies that the three highest doubly occupied molecular orbitals are almost degenerate with the three lowest unoccupied orbitals. This may suggest the absence of any π or δ bonding in spite of the short Fe–Fe distance which is close to that expected for a Fe–Fe double bond.[10]

The magnetic analysis for complex **1** is much more complicated, μ_{eff}, as a function of the temperature, shows an unusually slow linear decrease, and then a slower slight decrease, a sort of a plateau around 50 K, followed by a sudden decrease to zero as the temperature decreases from 50 to 2 K (Figure 8). Employing the above cited susceptibility equation for two coupled ions with $S = 2$ or ${}^3/_2$, even including zero-field terms in the spin Hamiltonian, we did not get any reasonable fit. The best results, however, have been obtained with a generalized Hamiltonian form

$$\hat{H}_S = E(S') + g\mu_B H\hat{S}'_z \qquad (11)$$

(where $S' = 0$–4 is the total spin, $\hat{S}'_z$ is the operator for the z component of the total spin, and H is the applied magnetic field) corresponding to a choice of independent energies for the singlet, triplet, quintet, septet, and nonet states with an isotropic Zeeman effect.[25] In such a model, the variable parameters are therefore the relative energies of the various states, $E(1)$, $E(2)$, $E(3)$, $E(4)$, g, and the monomeric impurity x. The corresponding susceptibility equation, obtained using the van Vleck formula,[26] is

$$\chi_{dim} = \frac{Ng^2\mu_B^2}{kT}\,\frac{2e^{-E(1)/kT} + 10e^{-E(2)/kT} + 28e^{-E(3)/kT} + 60e^{-E(4)/kT}}{1 + 3e^{-E(1)/kT} + 5e^{-E(2)/kT} + 7e^{-E(3)/kT} + 9e^{-E(4)/kT}} \qquad (12)$$

Its fitting to the experimental data gave $g = 1.9$, $E(1) = 25.7$, $E(2) = 213$, $E(3) = 552$, $E(4) > 1000$ cm^{-1}, $x = 2.3\%$, and $\theta = -0.87$ K. We wish to emphasize that the very high value of $E(4)$ gives a negligible contribution to the susceptibility. (The corresponding Boltzmann factor is negligible even at the highest considered temperature of 250 K.) Therefore the corresponding susceptibility equation for a $S = {}^3/_2$ dimer [eq 12 without the two exponential terms containing $E(4)$] fits the data as well.

In terms of the energy level pattern, the data analyzed thus far indicate that for complex **1** the $S = 4$ state is so high in energy that it is negligibly populated even at room temperature. Consequently, we can say that two of the unpaired electrons belonging to the iron atoms are essentially paired off (with an energy much greater than kT at room temperature, *i.e.* at least 3–4 kcal mol^{-1}). This could be due either to a very strong antiferromagnetic coupling through the mesityl bridge or to a direct Fe–Fe interaction. The high value of the corresponding coupling constant (which should be higher than -500 cm^{-1}) can hardly be explained by a superexchange through a carbon bridge and thus rules out the former possibility. On the other hand, the fairly short Fe–Fe distance [2.614(1) Å, to be compared with 2.48 Å in metallic iron] lies in the range expected for a single bond[10] and supports strongly a direct iron–iron interaction. However, a definitive conclusion on the existence of a localized σ Fe–Fe bond cannot be obtained from this magnetic analysis because of the small upper value of electron pairing energy detectable with such techniques (2–3 kcal mol^{-1}) which poses only a lower limit to the metal–metal interaction. The longer Fe–Fe distance with respect to complex **4** suggests a weaker iron–iron single bond which could be explained by a partial involvement of the iron d_σ orbital in a Fe–Mes axial bonding. This effect is well documented for example, in L'L$_4$MML$_4$L' complexes.[12] Moreover, we can stress the reasons of the Heisenberg model failure: the quintet state is much higher in energy than the triplet one and not to far from the septet one. This pattern is very different from that obtained by the Heisenberg Hamiltonian, $E(1) = 2J$, $E(2) = 6J$, $E(3) = 12J$, $E(4) = 20J$, where the energy levels are regularly separated, and explains the peculiar temperature dependence of the magnetic moment.

We analyze now the magnetic behavior of complexes **5**, **6**, and **8**–**10**, derived from the parent complexes **4** and **7**. The magnetic susceptibility data for **6** are quite consistent with its monomeric structure (Figure 4), showing a constant μ_{eff} value of 5.23 μ_B from 310 K down to 30 K. Such a result is typical for tetrahedral

(25) Cline, S. J.; Glerup, J.; Hodgson, D. J.; Jensen, G. S.; Pedersen, E. *Inorg. Chem.* **1981**, *20*, 2229.
(26) van Vleck, J. H. *The Theory of Electric and Magnetic Susceptibilities*; Oxford University: Oxford, U.K., 1932.

iron(II) compounds.[27] For complex **5**, the behavior of μ_{eff} as a function of temperature, with a μ_{eff} value of 5.19 μ_B almost constant down to 60 K, clearly indicates a monomeric structure. A best fit of this data, using the equation obtained taking into account the zero-field splitting through the Hamiltonian

$$H = gH\cdot\hat{S} + D[\hat{S}_z^2 - S(S+1)/3] \qquad (13)$$

for $S = 2$,[24] gives $g = 2.08$ and $D = 15.1$ cm^{-1} for complex **5** and $g = 2.07$ and $D = 8.1$ cm^{-1} for complex **6**, with all the parameters being as expected for iron(II) compounds.[27,28]

The dependence of μ_{eff} as a function of temperature for complexes **8** and **9** (Figures 9 and 10) closely resembles that for complex **7** (Figure 8). It has therefore been fitted with eq 10 for two exchange coupled ions with $S = 2$ obtaining $g = 2.30$, $J = -63.2$ cm^{-1}, $x = 2.1\%$, and $\theta = -8$ K for **8** and $g = 2.15$, $J = -58.7$ cm^{-1}, $x = 2.9\%$ and $\theta = -7$ K for **9**. Such parameters are very similar to those observed for complex **7** and suggest for complexes **8** and **9** the analogous dimeric structure.

The temperature-dependent magnetic susceptibility for **10** strongly indicates a change in the structure in comparison with the parent compound **7** (Figure 11). The temperature dependence of the magnetic moment shows a wide plateau, with μ_{eff} around 2.3 μ_B, between 50 and 200 K with a sudden decrease below 50 K and a slight increase at higher temperatures ($\mu_{eff} = 2.56$ μ_B at 310 K). Such a trend cannot be fit with any standard equation for two exchange coupled ions even including zero-field splitting and monomeric impurities. It has been successfully fitted using a model which considers the dimer as a single strongly coupled system with a triplet group state split by the spin–orbit coupling into singlet ($M_S = 0$) and doublet ($M_S = \pm 1$) component and a low lying quintet state. The magnetic susceptibility for such a system, obtained assuming that the singlet component lies lowest and using the van Vleck equation,[26] is

$$\chi_{dim} = \frac{Ng^2\mu_B^2}{kT}\,\frac{(2/3)e^{-D/kT} + (4kT/3D)(1-e^{-D/kT}) + 10e^{-\Delta_2/kT}}{1 + 2e^{-D/kT} + 5e^{-\Delta_2/kT}} \qquad (14)$$

where D is the zero-field splitting and Δ_2 is the separation between the lowest singlet component and the quintet state. A good fit was obtained for $g = 2.34$, $D = 12.8$ cm^{-1}, and $\Delta_2 = 556$ cm^{-1}, the g factor and the zero-field splitting values being in the range for iron(II) compounds.

Magnetostructural Correlations. The detailed analysis of the magnetic data prompted us to find a relationship between the magnetic results and the iron–iron distances at least for complexes **1**, **4**, and **7**, which have been structurally characterized. On the basis of our structural and magnetic results for complexes **1**, **4**, and **7**, can a relationship be stressed between the magnetic coupling within the dimeric unit, the iron–iron distance, and the existence of a metal–metal bond? Such a correlation can be made under the following conditions: (i) We should mention that there is a significant difference in the nature of the bridging ligands. (ii) For complex **1**, for which we used a model on the basis of eq 12, we can define an average coupling constant for the spin states up to $S = 3$ as

$$\bar{J} = -[E(1)/2 + E(2)/6 + E(3)/12]/3 \qquad (15)$$

thus the value is $\bar{J} = -31.5$ cm^{-1} (Table 12). (iii) For complex **7**, the temperature dependence of magnetic susceptibility below 300 K can actually be fitted using either a $S_1 = S_2 = 2$ (see above) or a $S_1 = S_2 = {}^3/_2$ binuclear susceptibility equation with identical results, since the $S = 4$ spin level is not significantly populated.

Table 12. Fe–Fe Distances (Å) and Coupling Constants (cm^{-1}) for Complexes **1**, **4**, and **7**

	R(Fe–Fe) (Å)	J (cm^{-1})
1	2.614(1)	−31.5
4	2.371(4)	−0.5
7	2.859(2)	−63.7

We are now in the position to compare the coupling constants of **1**, **4**, and **7** for the coupling of only three out of the four unpaired electrons on each Fe(II) center, the remaining one being either involved in a Fe–Fe σ bond, in complex **4** and very probably complex **1**, or someway strongly coupled, in complex **7**. The corresponding data are collected in Table 12. The coupling constant is inversely related to the iron–iron distance; it decreases as the metal–metal distance increases, becoming negligible in complex **4** which has the shortest iron–iron distance [2.371(4) Å]. This trend can be explained by admitting that the coupling of the three d_π and d_δ electrons through direct iron–iron interaction is negligible with respect to coupling through superexchange via bridging ligands, thus the magnitude of the coupling constants is determined only by the effectiveness of the bridging ligand to assist the electron exchange. Therefore, the dimeric μ-iminoacyl (complex **4**) is less effective, in this respect, than the μ-imino group (complex **7**), followed by the mesityl residue (complex **1**). Such a trend is expected on the basis of some very simple considerations.[29] This, in turn, is forseen to be lower in a biatomic –CN– bridge (see complex **4**) than in monoatomic –C– (complex **1**) or –N– bridges (complex **7**) and, between the two latter ones, higher for the –N– one.

Conclusions

Selective sequential insertion reactions led either to double functionalized or to differently functionalized iron–carbon bonds using [Fe_2Mes_4] as the starting compound. Thus, the difference in migratory aptitude of various iron–carbon bonds have been singled out. In addition, migratory insertion reactions into the iron–aryl bond in [Fe_2Mes_4] led to compounds, which, for the examples reported, constantly maintain the dimeric core with Fe···Fe distances varying from 2.317(4) to 2.859(2) Å. A careful analysis of the magnetic properties shed light on whether or not such distances correspond to the existence of a metal–metal bond. We were able to distinguish if the reduction of the magnetic moment arises from the metal–metal bond or from an antiferromagnetic coupling assisted by the bridging ligands. Rather unexpectedly, the shortest iron–iron distance in **4** [2.371(1) Å] corresponds to a very weak antiferromagnetic coupling, which becomes the more relevant coupling mechanism in **7** [Fe···Fe, 2.859(2) Å]. The nature (number and type of atoms) of the bridging ligand is essential in determining the type of antiferromagnetic coupling. The magnetic analysis pursued allowed us to assess the presence or not of a metal–metal bond within a class of closely related dimeric compounds of iron(II).

Experimental Section

General Procedure. All reactions were carried out under an atmosphere of purified nitrogen. Solvents were dried and distilled before use by standard methods. The modified synthesis of **1** is reported in detail. Infrared spectra were recorded with a Perkin-Elmer 883 spectrophotometer; ^{1}H NMR spectra were measured on a 200-AC Bruker instrument. Magnetic susceptibility measurements were made with a Quantum Design Model MPMS5 SQUID magnetometer operating at a magnetic field strength of 3 kOe, in the temperature range of 1.9–310 K. Corrections were applied for diamagnetism calculated from Pascal constants. Effective magnetic moments were calculated by the equation $\mu_{eff} = 2.828(\chi_{Fe}T)^{1/2}$, where χ_{Fe} is the magnetic susceptibility per atom atom. Fitting

(27) Casey, A. T.; Mitra, S. In *Theory and Applications of Molecular Paramagnetism*; Bodreaux, E. A., Mullay, L. N., Eds.; Wiley: New York, 1976; p 135.
(28) Carlin, L. R. *Magnetochemistry*; Springer: Berlin, Germany, 1986.
(29) Kahn, O. *Molecular Magnetism*; VCH: New York, 1993.

calculations of the experimental data to the theoretical equations were carried out using a Marquardt nonlinear least-squares fitting method, minimizing the function

$$F = \sum_i \frac{[\chi_i^{obsd} T_i - \chi_i^{calcd} T_i]^2}{(\chi_i^{obsd} T_i)^2}$$

Synthesis of 1. A THF solution of MesMgBr (147 mL, 1.021 M, 177.0 mmol) was added dropwise to a THF/dioxane (500/100 mL) suspension of $FeCl_2 \cdot (THF)_{1.5}$ (20.7 g, 88.3 mmol) at −30 °C, and then the suspension was warmed to room temperature and stirred for 2 h. The magnesium salts were removed by filtration. The solvent was evaporated to dryness and the solid residue very well dried. The solid was dissolved in Et_2O (500 mL) and the small amount of undissolved solid was removed by filtration. The red solution, when concentrated to 100 mL, allowed complex **1** to crystallize (52%). Anal. Calcd for $C_{36}H_{44}Fe_2$: C, 73.48; H, 7.54. Found: C, 73.20; H, 7.62. Complex **1** is thermally labile, so it should be kept at low temperature. It is very soluble in THF, Et_2O, and toluene, and only slightly soluble in *n*-hexane.

Synthesis of 2. A THF solution of 2,4,6-$Pr^iC_6H_2MgBr$ (164 mL, 1.12 M, 184.0 mmol) was added dropwise to a THF/dioxane (500/100 mL) suspension of $FeCl_2 \cdot (THF)_{1.5}$ (20.5 g, 87.5 mmol) and cooled to −30 °C. The suspension was warmed to room temperature and stirred for 2 h and then kept at 0 °C overnight. The magnesium salts were removed by filtration and the solvent evaporated to dryness. The solid residue was dissolved in Et_2O (500 mL) and the small amount of remaining solid removed. Complex **2** crystallized upon evaporation of Et_2O to 50–100 mL (43%) and was recrystallized from *n*-hexane. Crystals suitable for X-ray analysis were grown in benzene/hexane. Anal. Calcd for $C_{60}H_{92}Fe_2$: C, 77.90; H, 10.02. Found: C, 78.19; H, 10.15.

Synthesis of 3. A THF (130 mL) solution of **1** (1.54 g, 5.26 mmol) was cooled to −60 °C, and then pyridine (0.85 mL, 10.52 mmol) was added. The solution became instantly red-violet. The solution was warmed to room temperature and then concentrated to 20 mL. A crystalline red-violet solid, **3**, formed upon addition of 150 mL of Et_2O (58%). Anal. Calcd for $C_{28}H_{32}FeN_2$: C, 74.34; H, 7.31; N, 6.19. Found: C, 74.22; H, 7.17; N, 6.16.

Synthesis of 4. A THF (100 mL) solution of Bu^tNC (13.30 g, 39.4 mmol) was added dropwise to a THF (200 mL) solution of **1** (5.80 g, 19.7 mmol) at 0 °C. The solution was warmed to room temperature and stirred overnight. THF was completely evaporated and the residue dissolved in *n*-hexane (200 mL). Upon concentration, the solution gave black crystals of **4** (48.5%). Anal. Calcd for $C_{56}H_{80}Fe_2N_4$: C, 73.03; H, 8.76, N, 6.08. Found: C, 72.40; H, 8.80, N, 6.45. The solid used for the microanalysis was dried in vacuo and lost hexane of crystallization. Complex **4** formed independently of the Bu^tNC/Fe molar ratio employed (1:1 or 2:1). It is very sensitive to oxygen and moisture, but rather thermally stable. IR (nujol): 1601 (vs) cm^{-1}. The reaction of **3** with Bu^tNC gave **4**, regardless of the presence of pyridine.

Synthesis of 5. A THF (150 mL) solution of **4** (2.20 g, 4.90 mmol) was cooled to 0 °C and then saturated with CO_2. A sudden and abundant absorption of CO_2 was observed. The solution was warmed to room temperature and stirred for 2 days. The solvent was evaporated to dryness, and the residue, when treated with Et_2O, gave complex **5** as a yellow microcrystalline solid (65%). Anal. Calcd for $C_{30}H_{40}N_2O_4Fe$: C, 65.69; H, 7.35; N, 5.11. Found: C, 64.62; H, 7.35; N, 5.13. Complex **5** is well soluble in toluene and *n*-hexane, and slightly soluble in THF. IR (nujol): 1630 (vs), 1671 (vs) cm^{-1}. μ_{eff} = 5.19 μ_B at 310 K.

Synthesis of 6. A toluene (100 mL) solution of $(C_6H_{11})N{=}C{=}N(C_6H_{11})$ (0.82 g, 3.95 mmol) was added dropwise to a black toluene (120 mL) solution of **4** (0.91 g, 1.97 mmol) cooled at −30 °C. When the solution was warmed to room temperature and stirred for 2 days, it became deep red. The solvent was evaporated to dryness and the residue was dissolved in *n*-hexane, which gave, on standing, **6** as a red solid (36%). Anal. Calcd for $C_{54}H_{84}N_6Fe$: C, 74.28; H, 9.70; N, 9.63. Found: C, 74.22; H, 9.72; N, 9.66. IR (nujol): ν(C=N) 1567 (vs) cm^{-1}. μ_{eff} = 5.23 μ_B at 310 K.

Synthesis of 7. A toluene (100 mL) solution of PhCN (2.70 g, 26.70 mmol) was added dropwise to a toluene (150 mL) solution of **1** (3.90 g, 13.3 mmol) which was cooled to −30 °C. The solution was stirred overnight and then warmed to room temperature. Complex **7** crystallized upon concentration of the solution to 100 mL (55%). Anal. Calcd for $C_{64}H_{64}N_4Fe_2$: C, 76.80; H, 6.44; N, 5.60. Found: C, 76.83; H, 6.81; N, 5.82. The reaction always gave **7** regardless of the PhCN/**1** molar ratio employed. Complex **7** is fairly soluble in THF and slightly soluble in aromatic hydrocarbons. Crystal suitable for the X-ray analysis have been obtained from recrystallization in benzene. IR (nujol): ν(C=N) 2225, 1598, 1560 cm^{-1}.

Synthesis of 8. An Et_2O (70 mL) solution of $(C_6H_{11})N{=}C{=}N(C_6H_{11})$ (1.34 g, 6.47 mmol) was added dropwise to an Et_2O (150 mL) suspension of **7** (3.24 g, 6.47 mmol) cooled to −40 °C. The suspension, when warmed to room temperature and stirred overnight, gave a red solution, which was concentrated to 100 mL and cooled at 0 °C. Complex **8** formed as red crystals (67%). Anal. Calcd for $C_{76}N_{98}N_6Fe_2$: C, 75.61; H, 8.18; N, 6.96. Found: C, 74.59; H, 8.46; N, 6.94. IR (nujol): ν(C=N) 1610 (ws), 1571 (ws) cm^{-1}.

Synthesis of 9. A toluene (70 mL) solution of PhNCO (0.50 g, 4.24 mmol) was added dropwise to a toluene (150 mL) suspension of **7** (2.12 g, 4.24 mmol) cooled to −30 °C. The suspension, when warmed to room temperature and then stirred overnight, gave a solution which allowed complex **9** to precipitate, upon standing, as an orange-red solid (37%). Anal. Calcd for $C_{64}H_{64}N_4O_2Fe_2$: C, 74.42; H, 6.24; N, 5.42. Found: C, 74.27; H, 6.59; N, 5.68. IR (nujol): ν(CO, CN) 2255 (w), 1681.6 cm^{-1}.

Synthesis of 10. A toluene (100 mL) solution of Bu^tNC (0.81 g, 9.78 mmol) was added to a toluene (150 mL) suspension of **7** (4.89 g, 9.78 mmol) cooled to −40 °C. Upon stirring overnight and warming to room temperature, a deep red solution formed. Toluene was evaporated to 20 mL and then *n*-hexane was added (120 mL). The solution was stirred vigorously for 10 min and solid **10** began to form. The amount of solid was increased by a further concentration of the solution to 40 mL (57%). Anal. Calcd for $C_{60}H_{72}N_4Fe_2$: C, 74.99; H, 7.55; N, 5.83. Found: C, 74.87; H, 7.47; N, 6.36. IR (nujol) ν(C=N): 1603 (vs), 1571.2 (m) cm^{-1}.

X-ray Crystallography for Complexes 2–4, 6, and 7. The crystals selected for study were mounted in glass capillaries and sealed under nitrogen. The reduced cells were obtained with use of TRACER.[30] Crystal data and details associated with data collection are given in Tables 1 and SI. Data were collected at room temperature (295 K) on a single-crystal diffractometer. For intensities and background the profile measurement technique[31] was used. The structure amplitudes were obtained after the usual Lorentz and polarization corrections,[32] and the absolute scale was established by the Wilson method.[33] The crystal quality was tested by ψ scans showing that crystal absorption effects could be neglected for complexes **4** and **6**. The data for complexes **2**, **3**, and **7** were corrected for absorption using a semiempirical method.[34] The function minimized during the least-squares refinement was $\Sigma w|\Delta F|^2$. A weighting scheme based on counting statistics[32] was applied for all complexes. Anomalous scattering corrections were included in all structure factor calculations.[35b] Scattering factors for neutral atoms were taken from ref 35a for non-hydrogen atoms and from ref 36 for H. Among the low-angle reflections no correction was deemed necessary.

Solution and refinement were based on the observed reflections. The structures were solved by the heavy-atom method starting from a three-dimensional Patterson map for complexes **2**, **3**, **6**, and **7**. For **4** the structure was solved using SHELX86.[37] Refinements were done by full-matrix least-squares first isotropically and then anisotropically for all non-H atoms, except for the hexane solvent molecule in complex **4** and the C46–C48 methyl carbon atoms in complex **6**, which were found to be statistically distributed over two positions (A, B) and isotropically refined with site occupation factors of 0.55 and 0.45 for A and B positions, respectively. For **2**, **3**, **6**, and **7**, the hydrogen atoms were located from difference Fourier maps. For **4**, they were put in geometrically calculated positions. They were introduced in the subsequent refinements as fixed atom

(30) Lawton, S. L.; Jacobson, R. A. *TRACER (a cell reduction program)*; Ames Laboratory, Iowa State University of Science and Technology: Ames, IA, 1965.

(31) Lehmann, M. S.; Larsen, F. K. *Acta Crystallogr. Sec. A: Cryst. Phys. Diffr. Theor. Gen. Crystallogr.* **1974**, *A30*, 580–584.

(32) Data reduction, structure solution, and refinement were carried out on a GOULD 32/77 SHELX-76 computer using Sheldrick, G. *SHELX-76. System of Crystallographic Computer Programs*; University of Cambridge: Cambridge, England, 1976.

(33) Wilson, A. J. C. *Nature* **1942**, *150*, 151.

(34) North, A. C. T.; Phillips, D. C.; Mathews, F. S. *Acta Crystallogr., Sect. A: Cryst. Phys., Diffr., Theor. Gen. Crystallogr.* **1968**, *A24*, 351.

(35) *International Tables for X-ray Crystallography*; Kynoch Press; Birmingham, England, 1974; Vol. IV, (a) p 99, (b) p 149.

(36) Stewart, R. F.; Davidson, E. R.; Simpson, W. T. *J. Chem. Phys.* **1965**, *42*, 3175.

(37) Sheldrick, G. *SHELX-86: a FORTRAN-77 Program for the solution of Crystal Structure from Diffraction Data*; University of Cambridge: Cambridge; England, 1986.

contributions with isotropic U's fixed at 0.08 Å^2 for **6** and **7**, 0.10 Å^2 for **2** and **4**. For complex **3**, the isotropic U's were fixed at 0.06, 0.09, 0.15 Å^2 for the hydrogen associated to the benzene, pyridine, and methyl carbons, respectively. The H atoms associated to the benzene and *n*-hexane solvent molecules in complexes **2** and **4**, respectively, were ignored, as well as those related to the disordered methyl carbons in complex **6**. During the refinement of complexes **2**, **3**, and **7**, the Ph rings were constrained to be regular hexagons (C–C = 1.395 Å).

For complex **2** the low overdetermination ratio which is a consequence of the bad quality of the crystal, as well as of the intrinsic low scattering power possibly related to the vibrations of the isopropyl groups, reflects in the rather low accuracy of the structural analysis, clearly indicated by the high values of the esd's. Since the space group of complex **2** is polar, the crystal chirality was tested by inverting all the coordinates (x,y,z|$-x,-y,-z$) and refining to convergence again. The resulting R values (R = 0.057, R_G = 0.080 *vs* R = 0.058, R_G = 0.081) indicated that the original choice should be considered the correct one.

The final difference maps showed no unusual feature, with no significant peaks above the general background. Final atomic coordinates are listed in Tables 2–6 for non-H atoms and in Tables SII–SVI for hydrogens. Thermal parameters are given in Tables SVII–SXI, bond distances and angles in Tables SXII–SXVI.[38]

Acknowledgment. We thank the "Fonds National Suisse de la Recherche Scientifique" (Grant. No. 20-33420-92) and Ciba-Geigy Co. (Basel) for financial support.

Supplementary Material Available: Tables giving crystal data and details of the structure determination, bond lengths, bond angles, anisotropic thermal parameters, and hydrogen atom locations (21 pages); observed and calculated structure factors (40 pages). This material is contained in libraries on microfiche, immediately follows this article in the microfilm version of the journal, and can be ordered from the ACS; see any current masthead page for ordering information.

(38) See paragraph at the end of paper regarding supplementary material.